Am. J. Trop. Med. Hyg., 90(3), 2014, pp. 469–479
doi:10.4269/ajtmh.13-0051

Alteration of the Phenotypic and Pathogenic Patterns of *Burkholderia pseudomallei* that Persist in a Soil Environment

Yao-Shen Chen, Wun-Ju Shieh, Cynthia S. Goldsmith, Maureen G. Metcalfe, Patricia W. Greer, Sherif R. Zaki, Hsin-Hou Chang, Hao Chan, and Ya-Lei Chen*

Division of Infectious Diseases, Kaohsiung Veterans General Hospital, Kaohsiung, Taiwan; Graduate Institute of Science Education and Environmental Education, National Kaohsiung Normal University, Kaohsiung; Taiwan/Department of Internal Medicine, National Yang-Ming University, Taipei, Taiwan; Infectious Diseases Pathology Branch, Centers for Disease Control and Prevention, Atlanta, Georgia; Department of Molecular Biology and Human Genetics, Tzu-Chi University, Hualien, Taiwan; Institute of Medical Sciences, Tzu-Chi University, Hualien, Taiwan; Department of Biotechnology, National Kaohsiung Normal University, Kaoshiung, Taiwan

Abstract. Melioidosis is caused by the soil-borne pathogen *Burkholderia pseudomallei*. To investigate whether the distinct phenotypic and virulent characteristics result from environmental adaptations in the soil or from the host body, two pairs of isogenic strains were generated by passages in soil or mice. After cultivation in soil, the levels of 3-hydroxytetradecanoic acid, biofilm formation, flagellar expression, and ultrastructure were altered in the bacteria. Uniformly fatal melioidosis developed as a result of infection with mouse-derived strains; however, the survival rates of mice infected with soil-derived strains prolonged. After primary infection or reinfection with soil-derived strains, the mice developed a low degree of bacterial hepatitis and bacterial colonization in the liver and bone marrow compared with mice that were infected with isogenic or heterogenic mouse-derived strains. We suggest that specific phenotypic and pathogenic patterns can be induced through infection with *B. pseudomallei* that has been cultured in different (soil versus mouse) environments.

INTRODUCTION

Burkholderia pseudomallei is a soil-borne pathogen that is endemic to southeast Asia and northern Australia, and it can cause life-threatening infections (melioidosis).[1] The transmission of this disease occurs by subcutaneous inoculation, inhalation, or ingestion.[2] The clinical manifestations of melioidosis are variable but can include pneumonia with or without septicemia, multiple organ abscesses, localized subcutaneous inflammation, and asymptomatic melioidosis.[1] From the age of 4, many individuals have already had extensive and repeated contact with *B. pseudomallei* in endemic areas, and high titers of antibody against *B. pseudomallei* are detected in the serum of children.[3] Additionally, *B. pseudomallei* strains isolated from the same patient have distinct ribotypes after different infective episodes, suggesting that the patients reinfected with *B. pseudomallei* in endemic areas are very common.[4] Outbreaks of melioidosis with septicemia usually occur after extreme flooding events, such as heavy rain, cyclones, or typhoons.[5–7] Patients occasionally contract nonfatal subacute or chronic melioidosis during the dry season.[5] It is likely that the environmental *B. pseudomallei* load and virulence are increased after floods, although the host immune response also plays a role in the development of melioidosis.[5,8] To date, no reports have determined whether the virulence of *B. pseudomallei* is altered if the bacteria are dormant in a soil environment.

The lethality of *B. pseudomallei*-induced melioidosis in mice varies, and the infectious doses range from < 10 to $> 10^7$ colony-forming units (cfu). The required dose decreases after *in vivo* passage in BALB/c mice and increases in iron-deficient culture conditions.[9] The general virulence determinants, such as extracellular enzymes (protease, phospholipase, and catalase), biofilm formation, swarming ability, and lipopolysaccharide (LPS) types of different *B. pseudomallei* isolates are diverse.[10–12] The expression of one or more of these virulence determinants is associated with changes in bacterial colony morphology.[13–16] In *B. pseudomallei,* wrinkled and dry colonies are commonly observed in human isolates, and these morphologies are associated with the degree of virulence in BALB/c mice. Smooth and mucoid morphologies are more common to soil isolates and are less virulent.[10,17,18] We hypothesized that different phenotypic characteristics may result from native adaptations of the bacteria to different environments. Phenotypic characteristics, such as the production of extracellular enzymes, flagella, and different LPS types, may help the bacteria to survive dramatically different or harsh conditions, such as those found in the host or soil.

To address this issue, BALB/c mice were infected with *B. pseudomallei* that were previously passaged in mice or soil. The association between virulence and phenotypic differences of *B. pseudomallei* were investigated and discussed.

MATERIALS AND METHODS

Animals. BALB/c mice (females, 8 weeks old) were obtained from the Animal Laboratory Center (Taipei, Taiwan). All of the animal experiments in this study were approved by the Institutional Review Board of the National Kaohsiung Normal University (no. 9801), Taiwan. Care for all the animals was performed in accordance with the institutional guidelines.

Bacterial strains. *Burkholderia pseudomallei* vgh19 and *B. pseudomallei* CD were obtained from melioidosis patients or from soil environments.[19] From information on both strains, refer to the MLST (multilocus sequence typing) database (http://bpseudomallei.mlst.net/).[20] Mouse-derived *B. pseudomallei* strains NK19_mouse and NKcd_mouse were generated from the parent strains vgh19 and CD, respectively, by repeated intravenous injection into BALB/c mice. The injected bacteria ($\sim 10^5$ cfu/mL) were obtained from the supernatants of liver extracts (0.15 g of liver was homogenized using 1 mL phosphate buffered saline [PBS]). The soil-derived *B. pseudomallei* strains NK19_soil and NKcd_soil were generated from strains vgh19 and CD, respectively, and were maintained in sterile soil media. The soil medium was

*Address correspondence to Ya-Lei Chen, No. 62, Shen-Chung Rd., Yenchao, Kaohsiung 824. E-mail: dan1001@ms31.hinet.net

TABLE 1
Summary of soil characteristics in the media

Characteristics	Size, value, or concentration
Particles (mm)	< 0.002
pH*	6.9
Organic carbon (%)†	1.95%
Metal ion (mg/Kg)‡	
Cu	ND
Zn	38.3
Mn	14.9
Cr	ND
Ni	ND
Cd	ND
Pb	ND
Fe	190.2

*The pH was measured in a 1:2.5 soil:water suspension and electrical conductivity was determined using a saturation paste extract.
†The organic matter concentration was determined by the dichromate oxidation method.
‡The heavy metal content was analyzed by microwave extraction according to method 3051A of the United States Environmental Protection Agency (USEPA, 1998). The concentration was determined by flame (air-acetylene) atomic absorption spectroscopy (FAAS).
ND = not determined.

prepared from ~500 g of clay that was collected from a rice field. The general characteristics of the soil (particle size, pH, organic carbon, and metal ions) are summarized in Table 1. After autoclaving, the soil was dried in an oven (140°C, for 3 d) and mixed with sterile water (100 mL). The cycle of autoclaving the moist soil followed by drying it in an oven was repeated three times. Because high water content improves the growth of *B. pseudomallei*,[21] the moisture content of the soil media was adjusted to 12% using water containing 10^5 cfu/mL of bacteria. The water content of the soil was determined by subtracting the weight of the completely dry soil from the weight of the hydrated soil. After the appearance of different phenotypic characteristics (see below) of *B. pseudomallei* in soil media, ~1 g of soil was mixed with 3 mL of PBS, and the supernatant containing the bacteria (~10^5 cfu/mL) was separated by gravity precipitation to be used as infective sources. The specific growth constant (K) was derived from the equation $\ln N - \ln N_0 = K\,(t - t_0)$, where N represents the cell concentration per mL of a 5-hr culture (t), and N_0 represents the concentration of a 3-hr culture (t_0) at 37°C.[22]

Extracellular enzyme assay. The filtrates (< 0.45 μm, 100 μL) of the *B. pseudomallei* culture supernatants (3 mL) grown in LB (Luria broth) at 37°C for 24 hr were used for the detection of extracellular enzyme activity (U/mL).[12] One unit of protease activity was defined as an increase of 0.05 U/hr (540 nm) in a reaction solution (5 mg/mL of azocoll in 0.5 mL of 50 mM PBS, pH 7.5) that was incubated at 37°C for 16 hr. One unit of phospholipase C activity was defined as the amount of enzyme required to produce 1 μM of p-nitrophenol per minute in the reaction solution (20 mM p-nitrophenylphosphorylcholine in 250 mM Tris-HCl, pH 7.0, 60% glycerol (v/v) and 1 mM $ZnCl_2$). The catalase activity of the filtrates was determined using a catalase assay kit (Cayman Chem. Co., Ann Arbor, MI). The production of formaldehyde was measured spectrophotometrically at 405 nm with 4-amino-3-hydrazino- 5-mercapto-1,2,4-triazole.

Biofilm formation. Biofilm formation was assessed in a 96-well polyvinylchloride plate (BD Falcon; BD Biosciences, Bedford, MA).[23] Briefly, *B. pseudomallei* (10^8 cfu/mL; 100 μL) was seeded into 96-well plates and incubated for 20 hr at 37°C. The non-adhering planktonic cells were removed by washing with 100 μL of normal saline (0.9% [w/v] NaCl). The adhered cells were stained with 125 μL of crystal violet (1% [w/w], Pro-Laboratory Diagnostics, Richmond Hill, ON, Canada). After incubation for 20 min at room temperature, the excess crystal violet was removed by washing the plates with tap water. Finally, the bound crystal violet was released by adding 200 μL of 95% alcohol. The absorbance was measured at 595 nm using an Anthos 2010 microplate reader (Anthos Labtec Instruments GmbH, Wals, Salzburg, Austria).

Detection of 3-hydroxytetradecanoic acid. The fatty acid composition and the concentration of 3-hydroxytetradecanoic acid ($C_{14:0}$ 3-OH FA), a surrogate for LPS, was measured using an Agilent 6890 gas chromatograph/5973N mass selective detector system.[24] Briefly, *B. pseudomallei* was cultured in 10 mL of Vogel-Bonner medium (3.3 mM $MgSO_4$, 10 mM citric acid, 28 mM NaH_2PO_4, 37 mM K_2HPO_4, and 214 mM D-gluconic acid; pH 7.4) at 37°C for 7 d. The bacteria and culture supernatants were separated by filtration through a membrane (pore size of 0.45 μm). The filtrates were then lyophilized. The bacteria (~0.2 g) and filtrates were respectively suspended in 1 mL of methanolic NaOH (3.8 N) and then supplemented with an internal standard (30 μM deuterated $C_{14:0}$ FA), heated to 100°C in a cooled counter-flow system (30 min) and then adjusted with methanolic HCl (2.5 N) at 80°C (10 min). After esterification, hexane was added to form separate layers. The upper layer was removed, dried with nitrogen gas, and resuspended in 1 mL of hexane for gas chromatography-mass spectrometry (GC-MS) analysis. The GC was equipped with a 60-m DB23-MS (Agilent Technologies, Palo Alto, CA) capillary column (0.25-mm ID; 0.25-μm film thickness). The mass range was 50–550 m/z and was adapted to collect the full-scan mass spectra. Based on the ion intensity data from the full-scan mass spectra, the differentially fragmented ions (43/103/166 m/z) were used for identification and quantification. Standards (10–100 μM $C_{14:0}$ 3-OH FA, Sigma Chemical Co., St. Louis, MO) were used for calibration. The amount of 3-OH FA present in each sample, adjusted relative to the concentration of the recovered internal standard, was plotted against the ratio between the areas of the tested $C_{14:0}$ 3-OH FA and the areas of the standards.

Western blotting. The appearance of flagellin in the bacterial lysates was determined by immunoblotting[25]; a rabbit anti-flagellin polyclonal antibody was used for the primary reaction, and an anti-rabbit immunoglobulin G (IgG) conjugated with peroxidase was used for the secondary reaction. Enhanced chemiluminescent substrates (ECL, Thermo Fisher Scientific Inc., Rockford, IL) were added according to the manufacturer's instructions. The blots were developed using enhanced chemiluminescence (Millipore, Billerica, MA) and exposure to x-ray film.

Electron microscopy (EM). For scanning electron microscopy (SEM), bacteria were incubated on bovine serum albumin-precoated (1% w/v) coverslips for 15 min. Mouse- or soil-derived strains of *B. pseudomallei* were attached to the coverslips, fixed with 2.5% buffered glutaraldehyde, subjected to a series of alcohol dehydrations and critical point drying procedures, coated with gold, and observed under a Hitachi scanning electron microscope (Hitachi High-Technologies Co., Tokyo, Japan) at 15 kV (S-4700). For transmission electron microscopy (TEM), the bacteria or formalin-fixed tissues were washed in 0.1 M phosphate buffer, pH 7.3, and fixed in 2.5% buffered glutaraldehyde. The

specimens were collected, washed twice, post-fixed in 1% buffered osmium tetroxide, stained in 4% uranyl acetate, dehydrated with alcohol and propylene oxide, and then embedded in a mixture of epon resin (EM Sciences, Hatfield, PA). Thin sections (70 nm) were stained with 4% uranyl acetate and Reynolds's lead citrate. Sections were viewed at 80 kV using a Hitachi H-7500 transmission electron microscope fitted with a Gatan Multiscan 791 charge-coupled device camera. At least three different areas were randomly selected for photography at each magnification; representative data are shown. For negative stain preparations, glutaraldehyde-fixed specimens were resuspended in 4% buffered glutaraldehyde. Copper mesh grids coated with formvar and carbon (EM Sciences) were treated with Alcian blue and placed on drops of the specimen for 10 min, dried and stained with 2% phosphotungstic acid (pH 5.7).

Murine infection. The mice (N = 10 per group) were intravenously injected in the tail vein with 500 cfu of soil- (NK19_soil, NKcd_soil) or mouse- (NK19_mouse, NKcd_mouse) derived strains of *B. pseudomallei*. The mortality of the infected mice was recorded on Days 0–28. To initiate a second infection with *B. pseudomallei,* the mice (N = 10) were first infected with the soil-derived strain (NK19_soil or NKcd_soil). Then, 14 d post-infection, the infected mice were intravenously reinfected with *B. pseudomallei* (10 cfu; NK19_mouse or NK19_soil). At the indicated time, the mice were killed and the histological examination was performed. The liver enzymatic activity was assayed, and the inflammatory cytokines and bacterial colonization in the organs was measured (see below). Because most of the data derived from the primary infection experiments were identical, the representative data from the NK19_soil experiments are presented in this article.

Histology. The tissues of interest were excised, fixed in 4% formaldehyde, decalcified with 10% trichloroacetic acid (if the sample contained bone) and processed in paraffin wax embedding, using standard techniques. For the immunohistochemistry, colorimetric detection of the attached antibodies was performed using the Ultravision LP value Large Volume Detection System AP Polymer Kit (Thermo Fisher Scientific Inc., Rockford, IL) with rabbit polyclonal anti-*B. pseudomallei* antibodies. The antibody/polymer conjugate was visualized by applying Fast Red Chromogen dissolved in naphthol phosphate substrate buffer onto tissue sections for 20 min (Thermo Fisher Scientific Inc.).[26]

Liver functional enzymes. The levels of GOT (glutamic oxaloacetic transaminase) and GPT (glutamic pyruvic transaminase) were measured using a clinical biochemistry analysis system (COBAS INTEGRA 800, Roche, Basel, Switzerland).

Cytokine assay. Murine serum cytokines (tumor necrosis factor α [TNF-α], interleukin-6 [IL-6], interferon-gamma [IFN-γ], and IL-10) were measured using a Cytometric Bead Array Kit (CBA, BD Biosciences, San Diego, CA) according to the manufacturer's instructions. Briefly, a mixture of capture beads coated with specific antibodies (50 μL) conjugated to fluorophores with distinct fluorescence intensities (detected in Em, 423 nm) was combined with each serum sample (50 μL) or standard (50 μL). PE (phycoerythrin)-conjugated detection antibodies (detected in Em, 578 nm) were added to form the sandwich complex. After 2 hr at room temperature, the mixtures were washed and resuspended in 300 μL of wash buffer, and the signals were measured by flow cytometry (BD BiosystemsFACSCanto II system, BD Biosciences). The two-color cytometric data for the samples were analyzed using CBA software (Bender Medsystems, Burlington, CA), and standard curves were generated for each cytokine using the mixed cytokine/chemokine standard provided.

Bacterial loads. The bacterial loads in the liver and spleen were determined using a sequential weighing (liver, 0.25 g; spleen, 0.015 g), homogenization (1 mL PBS) and serial dilution protocol.[17] To determine the bacterial burdens in the bone marrow, one femur from each mouse was removed aseptically. The bone marrow was flushed with 1 mL PBS, and the number of bacteria was determined by plating serial dilutions. The limit of detection was 10 cfu/mL in the spleen (~670 cfu/g), the liver (~40 cfu/g) and bone marrow (~10 cfu/femur).

To estimate the amount of intracellular *B. pseudomallei*, the mononuclear cell layers of splenic cells were harvested by centrifugation (800 × *g*, 10 min) on a Ficoll-Hypaque (The Sigma Chemical Co.) density gradient. The red blood cells were lysed by treating with 0.83% NH_4Cl for 3 min and then rapidly buffering with PBS containing 2% fetal calf serum (FCS). The bone marrow cells were obtained from another femur by flushing with PBS. The collected cells were treated with PBS containing FCS (2%) and kanamycin (400 μg/mL) to remove any extracellular *B. pseudomallei*. After 1 hr, the cells (10^6 cell/mL) were harvested, lysed with sterile water (1 mL), and plated on an LB plate.

Statistical methods. The mean ± SD of the extracellular enzymatic activities (protease, phospholipase C, and catalase), biofilm formation and concentration of $C_{14:0}$ 3-OH fatty acids were calculated from independent cultures (N = 6, duplicate). The levels of the serum enzymes and cytokines as well as the number of bacteria colonizing the examined organs were averaged from individual mice (N = 6 for each group, duplicate). A significant difference was defined as $P < 0.05$ using the Mann-Whitney U test.

RESULTS

Altered phenotypic characterization. First, we evaluated whether certain phenotypic characteristics of *B. pseudomallei* were altered after they had been passaged in mice or in the soil (Table 2, summary of phenotypic characteristics of soil- and mouse-derived strains). The cellular extract from mouse-derived strains (NK19_mouse and NKcd_mouse) contained 59 fatty acid peaks that were distinguishable by GC-MS analysis. The fatty acids (FAs) that comprised the lipid A (endotoxin) component included $C_{16:0}$ 3-OH FA (3.64–3.9%), $C_{16:0}$ 2-OH FA (0.28–0.53%), $C_{14:0}$ 3-OH FA (5.17–5.46%), and $C_{14:0}$ 2-OH FA (0.52–0.77%). The production of $C_{14:0}$ 3-OH FA (an indicator of LPS) in the supernatants was higher and the biofilm formation on the plastic plate was lower in the mouse-derived strains as compared with the soil derived-strains. In the mouse-derived strains, the flagellin was constitutively expressed, and the colony morphology was wrinkly and dry on Ashdown's media (> 90%, counting 60 individual colonies). The soil-derived strains (NK19_soil and NKcd_soil) contained 42 distinguishable fatty acid peaks, including $C_{16:0}$ 3-OH FA (3.32–3.37%), $C_{16:0}$ 2-OH FA (0.26–0.32%), $C_{14:0}$ 3-OH FA (3.41–3.67%), and $C_{14:0}$ 2-OH FA (0.62–0.83%), within the cellular extracts. The production of $C_{14:0}$ 3-OH FA was relatively low, and biofilm formation was increased compared with the mouse-derived strains. Flagellin was not detected in bacteria obtained from the soil, however it was

TABLE 2
Summary of phenotypic characteristics of soil- and mouse-derived strains

	Burkholderia pseudomallei			
Strains	vgh19		CD	
Origins	Human		Soil	
MLST types*	ST1001		ST58	
Passages	Soil	Mouse	Soil	Mouse
Designation	NK19_soil	NK19_mouse	NKcd_soil	NKcd_mouse
	Phenotypic characteristics			
Specific growth constant (K)	0.94 ± 0.07	0.92 ± 0.05	0.98 ± 0.08	0.97 ± 0.06
Protease activity (U/mL)	7.5 ± 2.1	6.6 ± 1.4	9.0 ± 0.5	9.3 ± 1.6
Phospholipase C activity (U/mL)	23 ± 3.4	26 ± 1.7	19 ± 2.9	19 ± 1.2
Catalase activity (U/mL)	< 5	< 5	< 5	< 5
Fatty acid composition (%)†				
$C_{16:0}$ 3-OH FA	3.37	3.64	3.32	3.9
$C_{16:0}$ 2-OH FA	0.32	0.28	0.26	0.53
$C_{14:0}$ 3-OH FA	3.41	5.17	3.67	5.46
$C_{14:0}$ 2-OH FA	0.62	0.77	0.83	0.52
$C_{14:0}$ 3-OH FA (ng/mL)	27 ± 3.7	51 ± 3.4‡	33 ± 1.2	65 ± 3.4‡
Biofilm formation (optical unit)	0.7 ± 0.01	0.46 ± 0.05‡	0.83 ± 0.04	0.26 ± 0.07‡
Flagellin (immunoblotting)				
from isolates	+	+	–	+
in LB broth	+	+	+	+
Colony morphology	Mucoid	Dry-wrinkle	Mucoid	Dry-wrinkle

*ST58 prevail in Southeast Asia, ST1001 prevail in Taiwan (refer to http://bpseudomallei.mlst.net).[20]
†Major fatty acid (FA) compositions of lipid A (endotoxin) components of cellular extracts; percentages of the total fatty acid composition made up by the derivative of the named fatty acid.
‡Significance, $P < 0.05$ (compared between two isogenic strains).
MLST = multilocus sequence typing; LB = Luria broth.

detected in cultures of LB (Table 2, NKcd_soil). Approximately 70% of the soil-derived colonies ($N = 60$) exhibited a mucoid and smooth morphology. Growth rate and other phenotypic characteristics, such as the levels of protease, phospholipase C, and catalase in the supernatants were not shown to significant differences between the mouse- and soil-derived strains.

Ultrastructural PHB (polyhydroxybutyrate) particles were found intracellularly (Figure 1A), and capsules of the dividing cells were observed (Figure 1B). Finely pointed tips were observed on the surface of soil-derived strains (Figure 1C), whereas the same structure appeared as a round protrusion on the surface of mouse-derived strains (Figure 1D). Sparsely distributed, fragile and fine flagella (~0.005 μm) appeared exclusively on the surface of NKcd_soil strains (Figure 1E), whereas up to six robust flagella (0.0197 μm) were observed in most strains (Figure 1F). These results indicated that the distinct phenotypes of these strains were generated by incubation in different conditions (mouse versus soil).

Survival rate in murine melioidosis. We next determined whether the patterns of pathogenesis (survival rate, abscesses in organs, hepatitis, proinflammatory cytokine profile, and bacterial colonization in organs) were affected by the growth of *B. pseudomallei* in a mouse or soil environment. We had shown that intravenously injecting BALB/c mice with the parental strains (500 cfu, *B. pseudomallei* vgh19 or CD) resulted in fatal melioidosis within 2 or 3 d.[27] Thus, in this study, murine melioidosis ($N = 10$, each group) was induced by intravenous injection (500 cfu) of their offspring (isogenic mouse- and soil-derived strains). After infection with mouse-derived strains, all mice died within 4 d. In contrast, the mice infected with the soil-derived strains had a 40–50% survival rate on 28 d post-infection (Figure 2A).

In mice infected with soil-derived strains, clinical signs, including activity level, feeding, fur appearance and hunched posture, were severe 2 d post-infection but were partially mitigated after 4 d of infection. There was a possibility that the mice generated an immune response against the dissemination of *B. pseudomallei* in the bloodstream. To exclude this scenario, the surviving mice (Figure 2B, mice infected with NK19_soil; Figure 2C, mice infected with NKcd_soil) were

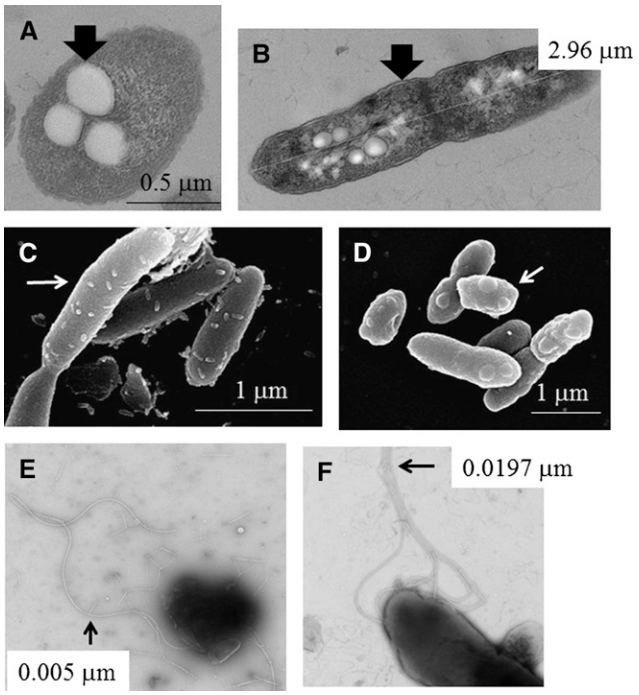

FIGURE 1. Ultrastructure of *Burkholderia pseudomallei.* The ultrastructure of the soil- and mouse-derived strains was observed by electron microscopy (EM), and representative images are shown. The arrows indicate the polyhydroxybutyrate (PHB) particles (**A**, NK19_mouse; transmission electron microscopy [TEM]), capsule (**B**, NK19_mouse; TEM), point tips (**C**, NK19_soil; scanning electron microscopy [SEM]), round protrusion (**D**, NK19_mouse; SEM), thin flagella (**E**, NKcd_soil; TEM, negative stain), and robust flagella (**F**, NK19_mouse; TEM, negative stain).

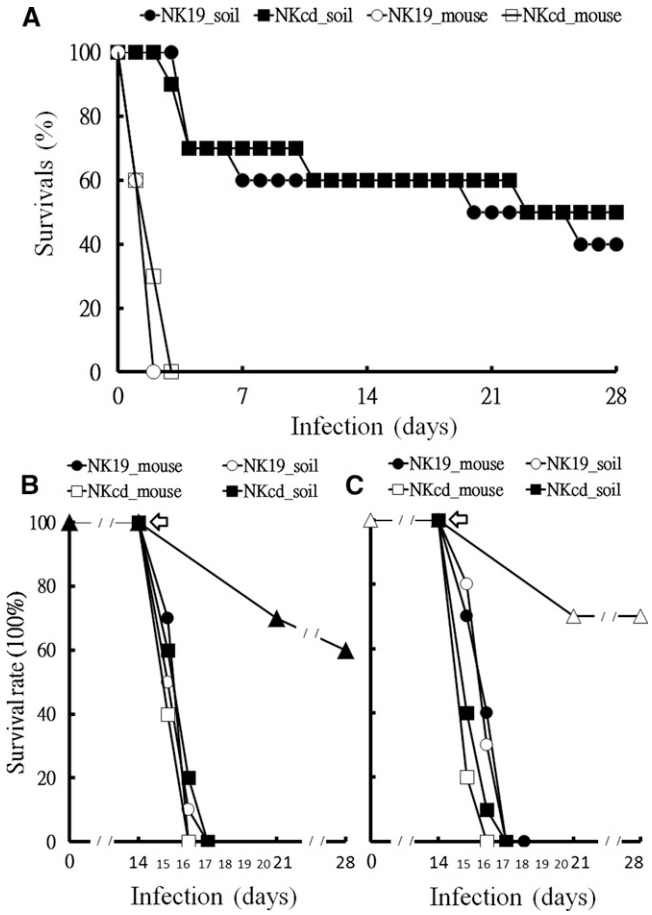

FIGURE 2. Survival rates after murine melioidosis. The mice that survived the intravenous injection of mouse-derived *B. pseudomallei* strains (500 cfu, NK19_mouse, white circles; 500 cfu, NKcd_mouse, white squares) and soil-derived *B. pseudomallei* strains (500 cfu, NK19_soil, black circles; 500 cfu, NKcd_soil, black squares) are shown (**A**). Mice that survived infection with NK19_soil (black triangle), (**B**) or NKcd_soil (white triangle), (**C**) (N = 10, 100%) were reinfected with *B. pseudomallei* (10 cfu, NK19_mouse, black circles; 10 cfu, NKcd_mouse, white squares; 10 cfu, NK19_soil, white circles; 10 cfu, NKcd_soil, black squares) by tail vein injection. The arrows indicate the day that the reinfection occurred.

reinfected by intravenous injection on Day 14 with a low dose (10 cfu) of isogenic or heterogenic mouse- or soil-derived strains. For example, if the primary infection was with the NK19_soil strain, the subsequent infection would be with the isogenic NK19_mouse (or NK19_soil) strain or a heterogenic NKcd_mouse (or NKcd_soil) strain. A low dose was used because we have previously showed that murine melioidosis cannot be established in BALB/c mice injected with < 10 cfu of *B. pseudomallei* vgh19 or CD (data not shown). However, despite the reinfection with isogenic or heterogenic mouse- or soil-derived strains, the condition of the infected mice rapidly deteriorated, and morbidity increased within 4 d. These results indicated that the mice that had experienced melioidosis were susceptible to reinfection with blood-borne *B. pseudomallei*.

Histological examination of murine melioidosis. We characterized the abscesses in organs that occurred during infection with the mouse- or soil-derived strains. In the observed group (infected with NK19_mouse; N = 6), no inflammation was found in the heart, kidneys, stomach, or intestines 2 d post-infection (data not shown). However, abscesses were found in the spleen (100%, 6 of 6), liver (100%, 6 of 6), bone marrow (50%, 3 of 6), and lung (33%, 2 of 6) (summarized in Table 3 and representative images shown in Figure 3A, spleen; Figure 3B, liver; Figure 3C, bone marrow; and Figure 3D, lung). The proportions of abscesses in each organ for the mice infected with the NKcd_mouse or parental strains (vgh19 and CD) were similar (N = 6 for each group). The occurrence of abscesses in the bone marrow was delayed for the mice infected with soil-derived strains (NKcd_soil and NK19_soil). The cellular necrotic foci were not observed on Day 2 but present in 100% of the mice infection after 6 d. In the mice infected with soil-derived strains, the abscesses in the spleen (100%, 6 of 6; for both strains), liver (100%, 6 of 6; for both strains), and lung (17%, 1 of 6; for NK19_soil and 33%, 2 of 6; for NKcd_soil) were observed on Day 2 post-infection (summarized in Table 3). In organs in which there were infected foci, the tissues contained a large number of *B. pseudomallei*-specific antigens from either the mouse- or soil-derived strains (a representative result is shown in Figure 3E, spleen; Figure 3F, liver; Figure 3G, bone marrow; and Figure 3H, lung). By EM examination, intact and replicating bacteria were observed intracellularly in hepatocytes after infection with mouse- or soil-derived strains (a representative result is shown in Figure 4A and B). These results suggested that the invading bacteria were present and replicating in the infected foci.

Murine melioidosis with hepatitis. Liver abscesses are commonly present during the progression of murine melioidosis.[17,27,28] In this study, we found that, on Day 2 post-infection, cellular necrosis was decreased in the livers of

TABLE 3
Summary of proportion of mice with abscesses

	Proportion of mice with abscesses in organs on Day 2 post-infection			
	Spleen	Liver	Bone marrow	Lung
Infection with				
Parent strains				
vgh19	100% (6/6)	100% (6/6)	66% (4/6)	33% (2/6)
CD	100% (6/6)	100% (6/6)	50% (3/6)	33% (2/6)
Mouse-derived strains				
NK19_mouse	100% (6/6)	100% (6/6)	50% (3/6)	33% (2/6)
NKcd_mouse	100% (6/6)	100% (6/6)	50% (3/6)	33% (2/6)
Soil-derived strains				
NK19_soil	100% (6/6)	100% (6/6)	0% (0/6)*	17% (1/6)
NKcd_soil	100% (6/6)	100% (6/6)	0% (0/6)*	33% (2/6)

*Shift to 100% (6/6) on Day 6 post-infection.

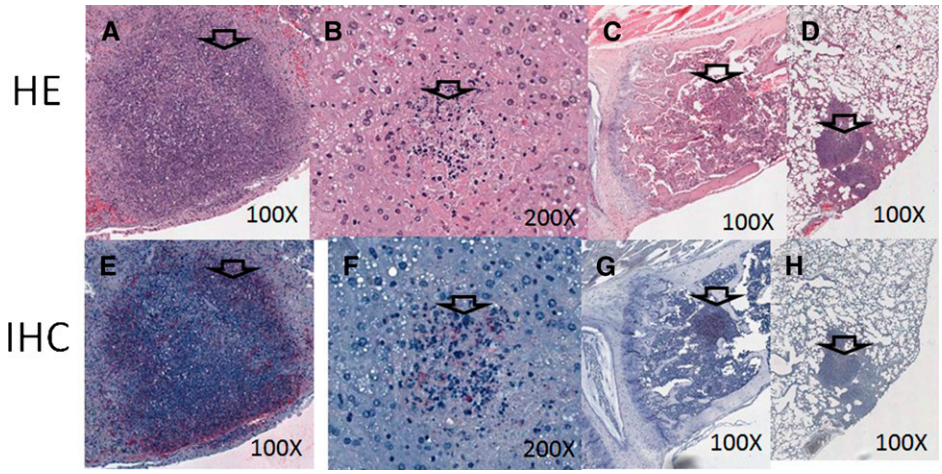

FIGURE 3. Histological examination. On Day 2 post-infection, the typical foci (indicated by arrows) in the spleen (**A**, **E**), liver (**B**, **F**), bone marrow (**C**, **G**), and lung (**D**, **H**) from murine melioidosis (a representative image of NK19_mouse infection) are shown by Hematoxylin and Eosin (H&E) stain (upper panels) and immunohistochemistry (bottom panels).

mice infected with soil-derived strains (Figure 5A) compared with mice infected with mouse-derived strains (Figure 5B). However, the levels of serum enzymes (GOT and GPT; $N = 6$ for each condition in duplicate) were not significant differences between mouse- and soil-derived strain infection (Figure 6A , GOT; Figure 6B, GPT). After infection with the soil-derived strains, the serum GOT and GPT levels were at maximal levels on Day 2 but then gradually decreased in the following days.

After primary infection, the infected mice were very susceptible to reinfection with *B. pseudomallei* by intravenous routes by 14 d post-infection (Figure 2B and C). Thus, those infected mice were induced severe hepatitis by secondary infection with isogenic strains (NK19_mouse and NK19_soil) or heterogenic strains (NKcd_mouse and NKcd_soil) ($N = 6$ for each condition, duplicate). The results indicated that severe hepatitis (> 1,000 IU/mL of GOP and GPT) was induced by mouse-derived strains but not by soil-derived strains (Figure 6, NK19_soil as representative of the primary infection). These patterns were reproducible when the NKcd_soil strain was used in the primary infection (data not shown).

Inflammatory cytokine response. It has been reported that an increase in the proinflammatory cytokines, TNF-α, IL-6, and IFN-γ, is associated with the severity of melioidosis.[29] In this study, the levels of these cytokines were shown to sharply up-regulate in all mice on Day 2 post-infection ($N = 6$ for each condition in duplicate; Figure 7A, TNF-α; Figure 7B, IL-6; Figure 7C, IFN-γ; Figure 7D, IL-10). At this time point, there was no significant difference in cytokine levels between infections with mouse- and soil-derived strains. However, when the mice were infected with a soil-derived strain and then reinfected with a mouse-derived strain on Day 14, the serum levels of TNF-α, IL-6, and IFN-γ were relatively higher compared with the cytokine profiles of mice reinfected with soil-derived strains.

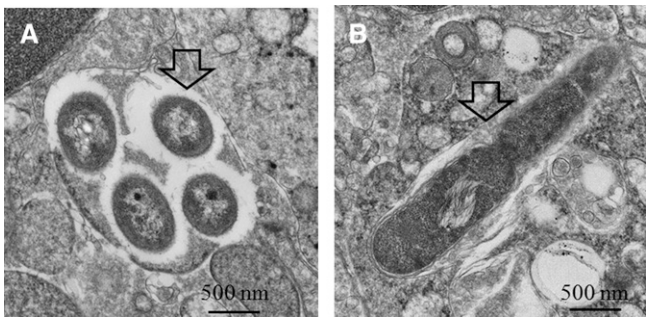

FIGURE 4. Observation by electron microscope. After infection with NK19_soil, the intracellular *B. pseudomallei* levels (**A**, arrow) and dividing bacteria (**B**, arrow) were observed in the liver by TEM (1:10,000×).

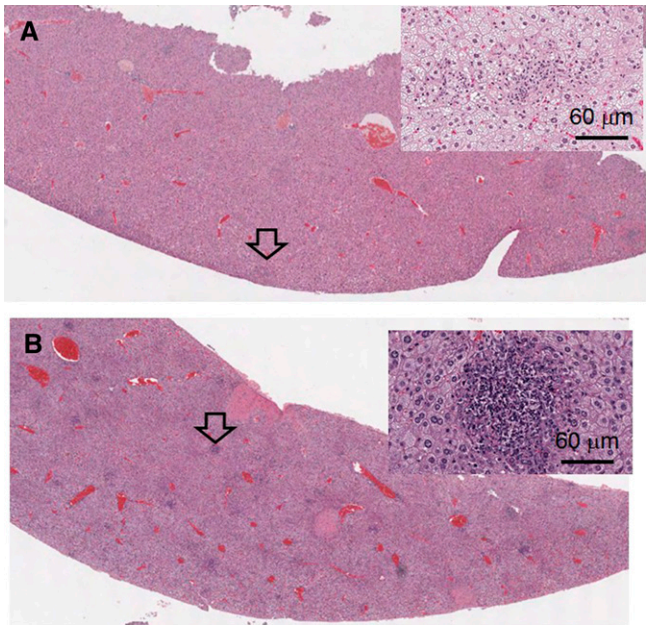

FIGURE 5. Liver abscess. Multiple foci from liver abscesses (arrows) were observed from mice infected with NK19_soil (**A**, Hematoxylin and Eosin [H&E]; 10×) or NK19_mouse (**B**, H&E; 10×). A high resolution (200×) image of representative foci is shown on the top right panel.

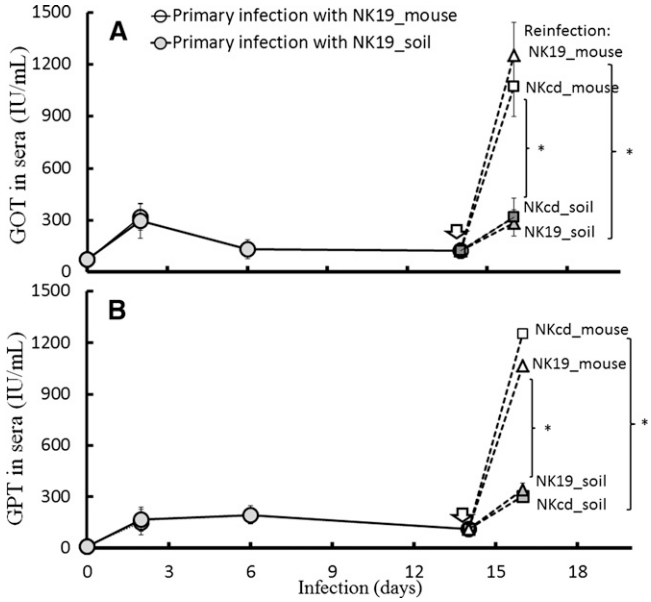

FIGURE 6. Liver functional enzymes. The levels of liver functional enzymes (**A**, glutamic oxaloacetic [GOT]; **B**, glumatic pyruvic transaminase [GPT]) in the sera of mice infected with NK19_mouse (as a representative of mouse-derived strains, white circles) or NK19_soil (as a representative of soil-derived strains, gray circles) were measured (N = 6, duplicate). After 2 d, no data were collected from the mice infected with NK19_mouse because all the mice died. After 14 d of primary infection with NK19_soil (arrows), the mice were reinfected with a mouse-derived strain (NK19_mouse, white triangles; NKcd_mouse, white squares) or a soil-derived strain (NK19_soil, gray triangles; NKcd_soil, gray squares).

Bacterial burden in organs. After primary infection, bacterial burden in spleen, liver, and bone marrow was found using mouse- or soil-derived strains (Figure 8A, for spleen; Figure 8B, for liver; Figure 8C, for bone marrow). As compared with the mice infected with soil-derived strains, on Day 2 post-infection, the numbers of bacterial colonization in liver were significantly higher in the mice infected with mouse-derived strains (Figure 8B). In the mice infected with soil-derived strains, no bacterial colonization in bone marrow occurred on Day 2 post-infection but were present on Day 6 and reached a plateau on Day 14 post-infection (Figure 8C).

As a result of secondary infection, bacterial colonization in liver and bone marrow were significantly increased in the mice reinfected with mouse-derived strains as compared with the mice reinfected with soil-derived strains (Figure 8B, liver; Figure 8C, bone marrow).

It is known that *B. pseudomallei* is capable of persisting in a variety of cell types.[30] Thus, the numbers of *B. pseudomallei* that persisted in splenic or bone marrow cells were measured (N = 6 for each condition in duplicate). In the mice infected with soil-derived strains, the number of bacteria that persisted in splenic cells reached a plateau early after infection (Figure 9A). However, in the bone marrow cells, intracellular *B. pseudomallei* was not found by 6 d infection but reached a peak on Day 14 post-infection (Figure 9B). In the reinfection model, the amount of intracellular bacteria present in the spleen after reinfection with mouse-derived strains was equal to the amount found after reinfection with soil-derived strains. The amount of intracellular bacteria in the bone marrow was significantly higher after infection with mouse-derived strains

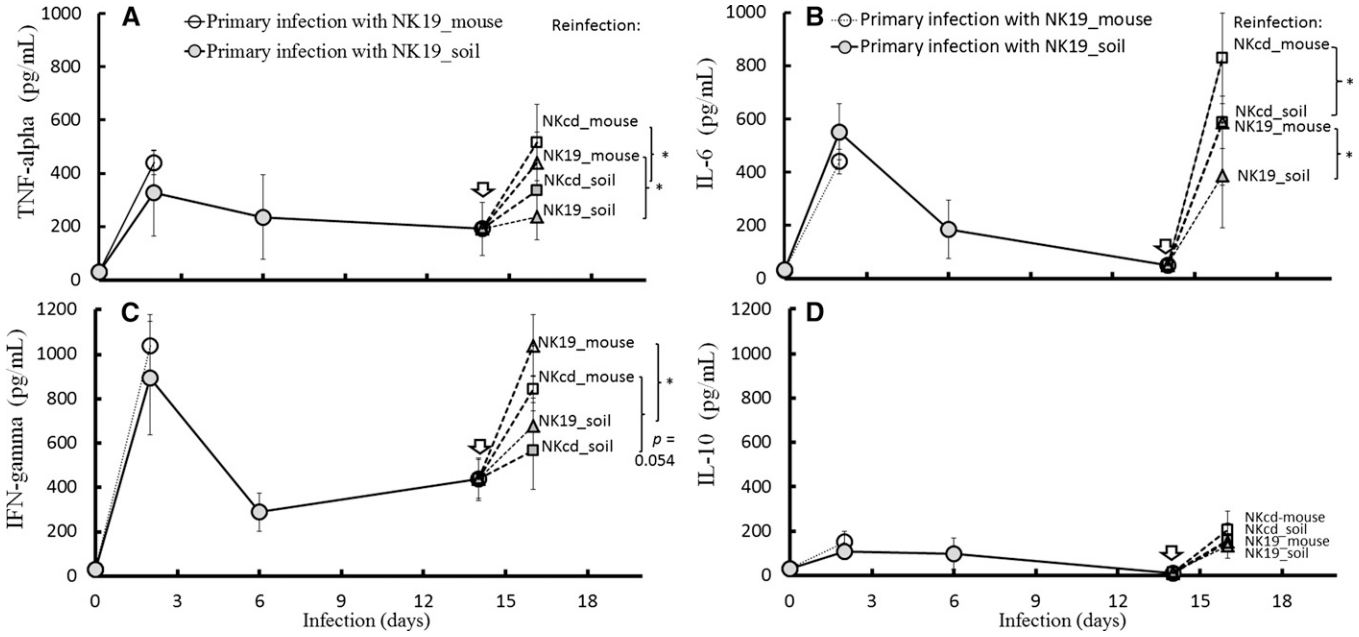

FIGURE 7. Serum cytokines. The levels of proinflammatory cytokines (**A**, tumor necrosis factor α [TNF-α]; **B**, interleukin-6 [IL-6]; **C**, interferon-gamma [IFN-γ]; **D**, IL-10) in the sera were measured (N = 6, duplicate) after primary infection with NK19_mouse (a representative of the mouse-derived strains, white circles) or NK19_soil (a representative of the soil-derived strains, gray circles). No data were collected after 2 d of infection with NK19_mouse because all the mice died. Fourteen days after infection with NK19_soil (arrows), the infected mice were reinfected with a mouse-derived strain (NK19_mouse, white triangles; NKcd_mouse, white squares) or a soil-derived strain (NK19_soil, gray triangles; NKcd_soil, gray squares). The results from another primary infection experiment (NKcd_mouse versus NKcd_soil) are not shown, as the pattern of altered cytokine expression in each reinfected condition was similar to the results shown (primary infection with NK19_mouse versus NK19_soil). The symbol (*) signifies $P < 0.05$.

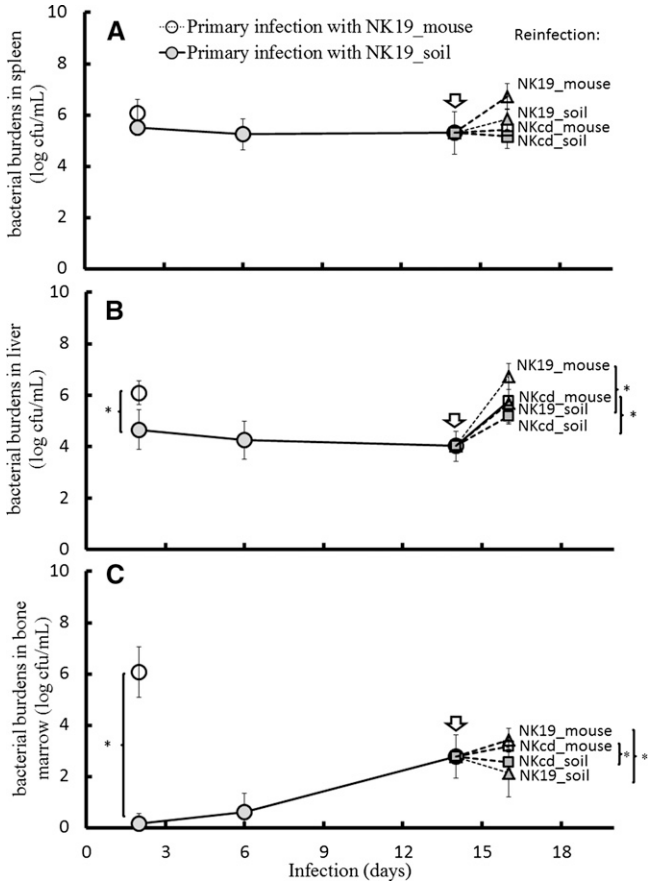

FIGURE 8. Bacterial burden in organs. The number of *Burkholderia pseudomallei* present in the spleen (**A**), liver (**B**), and bone marrow (**C**) were measured in mice infected with NK19_mouse (white circles) and NK19_soil (gray circles) on Day 2, Day 6, and Day 14 post-infection. Only one time point (Day 2 post-infection) is presented for the mice that were infected with NK19_mouse because all the mice died by Day 4 post-infection. Fourteen days after the primary infection with NK19_soil, the infected mice were reinfected with *B. pseudomallei* (NK19_mouse, white triangles; NKcd_mouse, white squares; NK19_soil, gray triangles; and NKcd_soil, gray squares). The data from the primary infection experiments using NKcd_mouse versus NKcd_soil are not shown because the pattern of bacterial burden in the organs for each condition was similar to the experiments shown (primary infection with NK19_mouse versus NK19_soil). The limit of detection was 10 cfu/ml in the spleen (~670 cfu/g), liver (~40 cfu/g), and bone marrow (~10 cfu/one femur). The symbol (*) signifies $P < 0.05$.

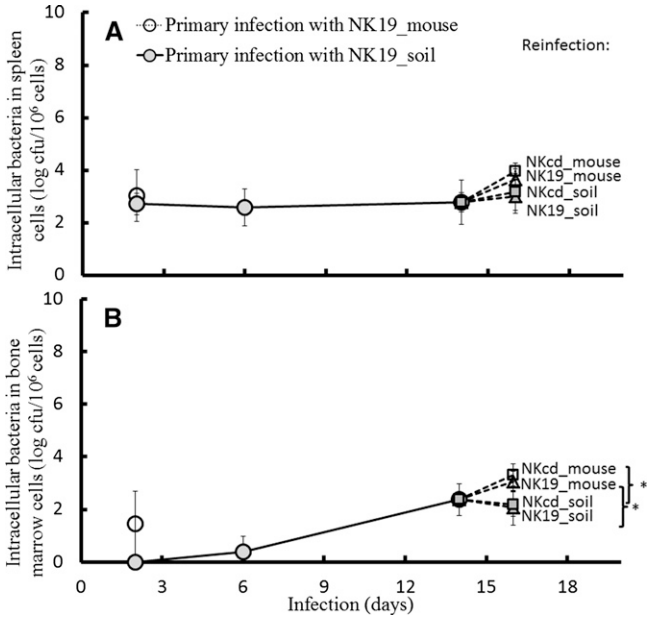

FIGURE 9. Intracellular bacteria in spleen and bone marrow cells. The levels of intracellular *Burkholderia pseudomallei* in the spleen (**A**) and bone marrow (**B**) were measured in the mice infected with NK19_mouse (white circles) and NK19_soil (gray circles) on Day 2, Day 6, and Day 14 post-infection. Only one point (Day 2 post-infection) is shown for the mice infected with NK19_mouse because all the mice died by d 4 post-infection. Fourteen days after infection with NK19_soil, the infected mice were reinfected with *B. pseudomallei* (NK19_mouse, white triangles; NKcd_mouse, white squares; NK19_soil, gray triangles; and NKcd_soil, gray squares). The data are not shown for another experiment (primary infection with NKcd_mouse versus NKcd_soil) because the levels of intracellular bacteria for each condition were similar to those shown (infection with NK19_mouse versus NK19_soil). The limit of detection for intracellular bacteria was 10 cfu/10^6 cells. The symbol (*) signifies $P < 0.05$.

compared with reinfection with soil-derived strains. Taken together, there is an altered pattern of pathogenesis when mice are infected with *B. pseudomallei* strains passaged in mice or obtained from soil.

DISCUSSION

Pre-existing conditions, such as diabetes mellitus, renal disease, or immunosuppression, have been recognized as important risk factors for melioidosis.[1] The inoculum size and virulence of *B. pseudomallei* are also important determinants that influence the severity of melioidosis.[8,9,31] Although melioidosis is a soil-borne disease, the relationship between adaption in different environments (soil versus host) and *B. pseudomallei* virulence remains to be elucidated. We and others have reported that intravenous injection of ~10^2 cfu of virulent *B. pseudomallei* originating from animals or humans was capable of inducing overexpression of TNF-α, IL-6, and IFN-γ, necrotic abscesses in the liver and spleen, and bacterial burden in liver, spleen, and bone marrow, and eventually develop fatal melioidosis within 4 d.[27,28] By contrast, in this study, after cultivation in soil, *B. pseudomallei* was attenuated to colonize in the bone marrow and induce hepatic abscesses. Consistently, the survival rates of mice were obviously prolonged. Although the clinical signs of murine melioidosis were partially mitigated in those mice, we found that numerous intracellularly replicating bacteria surrounded by hepatocyte phagosomal membranes, a result similar to that observed in mouse models of chronic melioidosis.[28] These bacteria-containing lesions may serve as reservoirs and allow for the rapid dissemination of *B. pseudomallei* under certain conditions. It has been demonstrated that no protective *B. pseudomallei*-specific IgG2a (Th1-related) antibodies was generated on Day 11 post-infection in a mouse model of bacteremic melioidosis.[28] In this study, regardless of the origin of the *B. pseudomallei* strain was used for reinfection, all infected mice eventually developed fatal melioidosis. This suggests that deleterious host responses induced by reinfection triggered the fatal effects. Phagocytic activity and IFN-γ production of leukocytes play crucial roles to reduce the early progression of melioidosis.[28,32–34] However, *B. pseudomallei* can still invade a variety of cells using flagella as cell-attachment

factors, and resist leukocytic oxidative burst activity by producing exopolysaccharides from capsules.[35,36] These phenotypic characteristics of flagellar and lipopolysaccharides of *B. pseudomallei* were significantly altered after adaption in soil environment. When compared with reinfection of soil-derived strains, reinfection of mouse-derived strains induced some degrees of exacerbated pathogenesis that included the subtle changes of elevated circulating proinflammatory cytokines (TNF-α, IL-6, and IFN-γ) and liver enzymes (GOP and GPT), as well as bacterial burden in liver and bone marrow. Both LPS and flagellin are the members of pathogen-associated molecular patterns and contribute to the induction of a cytokine storm and septic syndromes by toll-like receptor signaling.[37] It is not clear whether the alterations of the pathogenicity is also contributed by host response in response to phenotypic different bacteria. Probably various mechanisms are involved during primary and secondary infection, which eventually leads to different patterns of bacterial hepatitis, cytokine profile, and bacterial colonization in the liver or bone marrow.

Previous studies have found a high degree of diversity in the physical characteristics of *B. pseudomallei* isolates from different origins, including swarming ability, LPS structures, secretion of extracellular enzymes, biofilm formation, and colony morphology.[10–12,35,38–40] Even strains that originate from the same parental strain exhibit phenotypic diversity, particularly in colony morphology.[17,41] Both arginine deiminase and quorum sensing systems have been suggested to modulate the formation of colonies in response to different environmental conditions.[42–44] The genes involved in quorum sensing, phosphodiesterase, polyphosphate kinase, and LPS synthesis all contribute to biofilm formation, which plays a role in motility, stress sensing, and changes in colony morphology.[15,27,38,45–47] Because the colony morphology of *B. pseudomallei* was altered after growth in a soil environment, the morphology related characteristics, such as flagellin expression, concentration of $C_{14:0}$ 3-OH FA (a LPS indicator) and biofilm formation, which are also virulence determinants, might be similarly changed after growth in the environment. The $C_{14:0}$ 2-OH FA has been documented to be a feature that distinguishes virulent *B. pseudomallei* strains from non-virulent *Burkholderia thailandensis* strains.[48] After incubation in soil environments, no significant difference in the proportion of $C_{14:0}$ 2-OH FA in the total fatty acid composition was found among mouse- and soil-derived strains in this study. We showed that there were differences in the composition of many FAs, including the LPS indicator ($C_{14:0}$ 3-OH FA), and differences in biofilm formation and flagella between the mouse- and soil-derived strains. These phenotypic characteristics may be directly or indirectly involved in the alteration of *B. pseudomallei* pathogenicity. The observation that the *B. pseudomallei* phenotype and virulence were altered by growth in soil may partially explain the fact that *B. pseudomallei* isolated from different sources can exhibit dramatically different degrees of virulence.[31,39]

It has been reported that *B. pseudomallei* isolates cultured from multiple sites of a single patient with disseminated melioidosis show rapid changes in genotypic characteristics.[49] Other studies have shown that the irreversible alteration of the colony morphology of *B. pseudomallei* isolated from a water environment was accompanied by changes in the genetic background.[50] In this study, changes in the phenotypic characteristics associated with virulence could be induced by culturing the bacteria in a soil environment, but it is unknown whether these changes are reversible or permanent as a result of gene mutation.

In conclusion, the phenotypic characteristics ($C_{14:0}$ 3-OH FA, biofilm formation, flagellar expression, and ultrastructure) of *B. pseudomallei* were altered after incubation in a soil environment. In addition, the survival rate and pathogenic patterns (development of bacterial hepatitis, inflammatory cytokine levels, and bacterial colonization in the liver and bone marrow) in mice were changed after primary infection or reinfection with isogenic or heterogenic soil-derived strains. Our study indicates that the virulent alteration of *B. pseudomallei* may result from native adaptations of the bacteria to different (soil versus mouse) environments.

Received January 25, 2013. Accepted for publication December 16, 2013.

Published online January 20, 2014.

Financial support: This work was supported by grants NSC 99-2320-B-017-002-MY3, NSC99-2320-B-075B-001-MY3, VGHKS102-016, and VGHKS99-038.

Authors' addresses: Yao-Shen Chen, Division of Infectious Diseases, Kaohsiung Veterans General Hospital, Kaohsiung, Taiwan, Graduate Institute of Science Education and Environmental Education, National Kaohsiung Normal University, Kaohsiung, Taiwan, and Department of Internal Medicine, National Yang-Ming University, Taipei, Taiwan, E-mail: dan1001@ms31.hinet.net. Wun-Ju Shieh, Centers for Disease Control and Prevention, Infectious Diseases Pathology Branch, Atlanta, GA, E-mail: WShieh@cdc.gov. Cynthia S. Goldsmith, Maureen G. Metcalfe, Patricia W. Greer, and Sherif R. Zaki, Centers for Disease Control and Prevention, Infectious Disease and Pathology Activity, Atlanta, GA, E-mails: csg1@cdc.gov, gnf3@cdc.gov, pwg1@cdc.gov, and sxz1@cdc.gov. Hsin-Hou Chang and Hao Chan, Tzu-Chi University, Department of Molecular Biology and Human Genetics, Hualien, Taiwan, E-mail: hhchang@mail.tcu.edu.tw and b_pseudo@yahoo.com.tw. Ya-Lei Chen, National Kaohsiung Normal University, Biotechnology, Yenchao, Kaohsiung, Taiwan, E-mail: dan1001@ms31.hinet.net.

REFERENCES

1. Cheng AC, Currie BJ, 2005. Melioidosis: epidemiology, pathophysiology, and management. *Clin Microbiol Rev 18:* 383–416.
2. Limmathurotsakul D, Kanoksil M, Wuthiekanun V, Kitphati R, deStavola B, Day NP, Peacock SJ, 2013. Activities of daily living associated with acquisition of melioidosis in northeast Thailand: a matched case-control study. *PLoS Negl Trop Dis 7:* e2072.
3. Wuthiekanun V, Chierakul W, Langa S, Chaowagul W, Panpitpat C, Saipan P, Thoujaikong T, Day NP, Peacock SJ, 2006. Development of antibodies to *Burkholderia pseudomallei* during childhood in melioidosis-endemic northeast Thailand. *Am J Trop Med Hyg 74:* 1074–1075.
4. Maharjan B, Chantratita N, Vesaratchavest M, Cheng A, Wuthiekanun V, Chierakul W, Chaowagul W, Day NP, Peacock SJ, 2005. Recurrent melioidosis in patients in northeast Thailand is frequently due to re-infection rather than relapse. *J Clin Microbiol 43:* 6032–6034.
5. Currie BJ, Jacups SP, 2003. Intensity of rainfall and severity of melioidosis, Australia. *Emerg Infect Dis 9:* 1538–1542.
6. Su HP, Yang HW, Chen YL, Ferng TL, Chou YL, Chung TC, Chen CH, Chiang CS, Kuan MM, Lin HH, Chen YS, 2007. Prevalence of melioidosis in the Er-Ren River Basin, Taiwan: implications for transmission. *J Clin Microbiol 45:* 2599–2603.
7. Inglis TJ, O'Reilly L, Merritt AJ, Levy A, Heath CH, 2011. The aftermath of the Western Australian melioidosis outbreak. *Am J Trop Med Hyg 84:* 851–857.
8. Wiersinga WJ, van der Poll T, White NJ, Day NP, Peacock SJ, 2006. Melioidosis: insights into the pathogenicity of *Burkholderia pseudomallei*. *Nat Rev Microbiol 4:* 272–282.

9. Ulett GC, Currie BJ, Clair TW, Mayo M, Ketheesan N, Labrooy J, Gal D, Norton R, Smith CA, Barnes J, Warner J, Hirst RG, 2001. *Burkholderia pseudomallei* virulence: definition, stability and association with clonality. *Microbes Infect 3:* 621–631.
10. Chantratita N, Wuthiekanun V, Boonbumrung K, Tiyawisutsri R, Vesaratchavest M, Limmathurotsakul D, Chierakul W, Wongratanacheewin S, Pukritiyakamee S, White NJ, Day NP, Peacock S, 2006. Biological relevance of colony morphology and phenotypic switching by *Burkholderia pseudomallei*. *J Bacteriol 189:* 807–817.
11. Sawasdidoln C, Taweechaisupapong S, Sermswan RW, Tattawasart U, Tungpradabkul S, Wongratanacheewin S, 2010. Growing *Burkholderia pseudomallei* in biofilm stimulating conditions significantly induces antimicrobial resistance. *PLoS ONE 5:* e9196.
12. Vellasamy KM, Vasu C, Puthucheary SD, Vadivelu J, 2009. Comparative analysis of extracellular enzymes and virulence exhibited by *Burkholderia pseudomallei* from different sources. *Microb Pathog 47:* 111–117.
13. Mann EE, Wozniak DJ, 2012. Pseudomonas biofilm matrix composition and niche biology. *FEMS Microbiol Rev 36:* 893–916.
14. Choi KS, Veeraragouda Y, Cho KM, Lee SO, Jo GR, Cho K, Lee K, 2007. Effect of gacS and gacA mutations on colony architecture, surface motility, biofilm formation and chemical toxicity in *Pseudomonas* sp. KL28. *J Microbiol 45:* 492–498.
15. Yan Q, Hu X, Wang N, 2012. The novel virulence-related gene nlxA in the lipopolysaccharide cluster of *Xanthomonas citri* ssp. citri is involved in the production of lipopolysaccharide and extracellular polysaccharide, motility, biofilm formation and stress resistance. *Mol Plant Pathol 13:* 923–934.
16. Subramoni S, Nguyen DT, Sokol PA, 2011. *Burkholderia cenocepacia* ShvR-regulated genes that influence colony morphology, biofilm formation, and virulence. *Infect Immun 79:* 2984–2997.
17. Chen YS, Lin HH, Hung CC, Mu JJ, Hsiao YS, Chen YL, 2009. Phenotypic characteristics and pathogenic ability across distinct morphotypes of *Burkholderia pseudomallei* DT. *Microbiol Immunol 53:* 184–189.
18. Palasatien S, Lertsirivorakul R, Royros P, Wongratanacheewin S, Sermswan RW, 2008. Soil physicochemical properties related to the presence of *Burkholderia pseudomallei*. *Trans R Soc Trop Med Hyg 102 (Suppl 1):* S5–S9.
19. Chen YS, Lin HH, Mu JJ, Chiang CS, Chen CH, Buu LM, Lin YE, Chen YL, 2010. Distribution of melioidosis cases and viable *Burkholderia pseudomallei* in soil: evidence for emerging melioidosis in Taiwan. *J Clin Microbiol 48:* 1432–1434.
20. Chen YL, Lin YC, Chen YS, Chen SC, Liu YM, Tseng IL, Chiang CS, Lin HH, Mu JJ, 2013. Characterization of predominant molecular patterns of *Burkholderia pseudomallei* in Taiwan. *Trans R Soc Trop Med Hyg 107:* 165–169.
21. Inglis TJ, Sagripanti JL, 2006. Environmental factors that affect the survival and persistence of *Burkholderia pseudomallei*. *Appl Environ Microbiol 72:* 6865–6875.
22. Chen YS, Chen SC, Kao CM, Chen YL, 2003. Effects of soil pH, temperature and water content on the growth of *Burkholderia pseudomallei*. *Folia Microbiol (Praha) 48:* 253–256.
23. Mima T, Schweizer HP, 2010. The BpeAB-OprB efflux pump of *Burkholderia pseudomallei* 1026b does not play a role in quorum sensing, virulence factor production, or extrusion of aminoglycosides but is a broad-spectrum drug efflux system. *Antimicrob Agents Chemother 54:* 3113–3120.
24. Chen YS, Lin HH, Liu PJ, Tsai HY, Hsueh PT, Liu HY, Chen YL, 2011. Use of 3-hydroxy fatty acid concentrations in a murine air pouch infection model as a surrogate marker for LPS activity: a feasibility study using environmental *Burkholderia cenocepacia* isolates. *J Microbiol Methods 87:* 368–374.
25. Chen YS, Shiuan D, Chen SC, Chye SM, Chen YL, 2003. Recombinant truncated flagellin of *Burkholderia pseudomallei* as a molecular probe for diagnosis of melioidosis. *Clin Diagn Lab Immunol 10:* 423–425.
26. Guarner J, Zaki SR, 2006. Histopathology and immunohistochemistry in the diagnosis of bioterrorism agents. *J Histochem Cytochem 54:* 3–11.
27. Chen YL, Chen YS, Chan H, Tseng YH, Yang SR, Tsai HY, Liu HY, Sun DS, Chang HH, 2012. The use of nanoscale visible light-responsive photocatalyst TiO2-Pt for the elimination of soil-borne pathogens. *PLoS ONE 7:* e31212.
28. Hoppe I, Brenneke B, Rohde M, Kreft A, Häussler S, Reganzerowski A, Steinmetz I, 1999. Characterization of a murine model of melioidosis: comparison of different strains of mice. *Infect Immun 67:* 2891–2900.
29. Simpson AJ, Smith MD, Weverling GJ, Suputtamongkol Y, Angus BJ, Chaowagul W, White NJ, van Deventer SJ, Prins JM, 2000. Prognostic value of cytokine concentrations (tumor necrosis factor-alpha, interleukin-6, and interleukin-10) and clinical parameters in severe melioidosis. *J Infect Dis 181:* 621–625.
30. Jones AL, Beveridge TJ, Woods DE, 1996. Intracellular survival of *Burkholderia pseudomallei*. *Infect Immun 64:* 782–790.
31. Ulett GC, Labrooy JT, Currie BJ, Barnes JL, Ketheesan N, 2005. A model of immunity to *Burkholderia pseudomallei*: unique responses following immunization and acute lethal infection. *Microbes Infect 7:* 1263–1275.
32. Barnes JL, Ulett GC, Ketheesan N, Clair T, Summers PM, Hirst RG, 2001. Induction of multiple chemokine and colony-stimulating factor genes in experimental *Burkholderia pseudomallei* infection. *Immunol Cell Biol 79:* 490–501.
33. Srisurat N, Sermswan RW, Tatawasart U, Wongratanacheewin S, 2010. Bacterial loads and antibody responses in BALB/c mice infected with low and high doses of *Burkholderia pseudomallei*. *Am J Trop Med Hyg 82:* 1102–1105.
34. Santanirand P, Harley VS, Dance DA, Drasar BS, Bancroft GJ, 1999. Obligatory role of gamma interferon for host survival in a murine model of infection with *Burkholderia pseudomallei*. *Infect Immun 67:* 3593–3600.
35. Warawa JM, Long D, Rosenke R, Gardner D, Gherardini FC, 2009. Role for the *Burkholderia pseudomallei* capsular polysaccharide encoded by the wcb operon in acute disseminated melioidosis. *Infect Immun 77:* 5252–5261.
36. Galyov EE, Brett PJ, DeShazer D, 2010. Molecular insights into *Burkholderia pseudomallei* and *Burkholderia mallei* pathogenesis. *Annu Rev Microbiol 64:* 495–517.
37. Ferstl R, Spiller S, Fichte S, Dreher S, Kirschning CJ, 2009. Experimental models of acute infection and Toll-like receptor driven septic shock. *Methods Mol Biol 517:* 313–327.
38. Lee HS, Gu F, Ching SM, Lam Y, Chua KL, 2010. CdpA is a *Burkholderia pseudomallei* cyclic di-GMP phosphodiesterase involved in autoaggregation, flagellum synthesis, motility, biofilm formation, cell invasion, and cytotoxicity. *Infect Immun 78:* 1832–1840.
39. Lee SH, Chong CE, Lim BS, Chai SJ, Sam KK, Mohamed R, Nathan S, 2007. *Burkholderia pseudomallei* animal and human isolates from Malaysia exhibit different phenotypic characteristics. *Diagn Microbiol Infect Dis 58:* 263–270.
40. Tuanyok A, Stone JK, Mayo M, Kaestli M, Gruendike J, Georgia S, Warrington S, Mullins T, Allender CJ, Wagner DM, Chantratita N, Peacock SJ, Currie BJ, Keim P, 2012. The genetic and molecular basis of O-antigenic diversity in *Burkholderia pseudomallei* lipopolysaccharide. *PLoS Negl Trop Dis 6:* e1453.
41. Tandhavanant S, Thanwisai A, Limmathurotsakul D, Korbsrisate S, Day NP, Peacock SJ, Chantratita N, 2010. Effect of colony morphology variation of *Burkholderia pseudomallei* on intracellular survival and resistance to antimicrobial environments in human macrophages *in vitro*. *BMC Microbiol 10:* 303.
42. Chantratita N, Tandhavanant S, Wikraiphat C, Trunck LA, Rholl DA, Thanwisai A, Saiprom N, Limmathurotsakul D, Korbsrisate S, Day NP, Schweizer HP, Peacock SJ, 2012. Proteomic analysis of colony morphology variants of *Burkholderia pseudomallei* defines a role for the arginine deiminase system in bacterial survival. *J Proteomics 75:* 1031–1042.
43. Eberl L, 2006. Quorum sensing in the genus *Burkholderia*. *Int J Med Microbiol 296:* 103–110.
44. Gupta R, Schuster M, 2012. Quorum sensing modulates colony morphology through alkyl quinolones in *Pseudomonas aeruginosa*. *BMC Microbiol 12:* 30.
45. Gamage AM, Shui G, Wenk MR, Chua KL, 2011. N-Octanoylhomoserine lactone signaling mediated by the BpsI-BpsR quorum sensing system plays a major role in biofilm formation of *Burkholderia pseudomallei*. *Microbiology 157:* 1176–1186.

46. Tunpiboonsak S, Mongkolrob R, Kitudomsub K, Thanwatanaying P, Kiettipirodom W, Tungboontina Y, Tungpradabkul S, 2010. Role of a *Burkholderia pseudomallei* polyphosphate kinase in an oxidative stress response, motilities, and biofilm formation. *J Microbiol 48:* 63–70.
47. Ulrich RL, Deshazer D, Brueggemann EE, Hines HB, Oyston PC, Jeddeloh JA, 2004. Role of quorum sensing in the pathogenicity of *Burkholderia pseudomallei*. *J Med Microbiol 53:* 1053–1064.
48. Novem V, Shui G, Wang D, Bendt AK, Sim SH, Liu Y, Thong TW, Sivalingam SP, Ooi EE, Wenk MR, Tan G, 2009. Structural and biological diversity of lipopolysaccharides from *Burkholderia pseudomallei* and *Burkholderia thailandensis*. *Clin Vaccine Immunol 16:* 1420–1428.
49. Price EP, Hornstra HM, Limmathurotsakul D, Max TL, Sarovich DS, Vogler AJ, Dale JL, Ginther JL, Leadem B, Colman RE, Foster JT, Tuanyok A, Wagner DM, Peacock SJ, Pearson T, Keim P, 2010. Within-host evolution of *Burkholderia pseudomallei* in four cases of acute melioidosis. *PLoS Pathog 6:* e1000725.
50. Pumpuang A, Chantratita N, Wikraiphat C, Saiprom N, Day NP, Peacock SJ, Wuthiekanun V, 2011. Survival of *Burkholderia pseudomallei* in distilled water for 16 years. *Trans R Soc Trop Med Hyg 105:* 598–600.